Supplement Material for

Transcontinental Transport of a massive SO_2 plume from the Tehran Refinery Explosion in March 2026 Observed from Space

Shangyi Liu[1,2], Cathy Clerbaux[2,3], Anne Boynard[2,4], Mingjian Gu[5], Chengli Qi[6], Bruno Franco[3], Lieven Clarisse[3], Shan Han[1], Mengya Sheng[1], Nicolas Theys[7], Zhao-Cheng Zeng[1,*]

[1] School of Earth and Space Sciences, Peking University, Beijing, China
[2] LATMOS/IPSL, Sorbonne Université, UVSQ, CNRS, Paris, France
[3] Université libre de Bruxelles (ULB), BLU-ULB research Center, Spectroscopy, Quantum Chemistry and Atmospheric Remote Sensing (SQUARES), Brussels, Belgium
[4] SPASCIA, Ramonville-Saint-Agne, Toulouse, France
[5] Shanghai Institute of Technical Physics, Chinese Academy of Sciences, Shanghai, China
[6] National Satellite Meteorological Center, China Meteorological Administration, Beijing, China
[7] Royal Belgian Institute for Space Aeronomy (BIRA-IASB), Brussels, Belgium

Correspondence to: Zhao-Cheng Zeng (zczeng@pku.edu.cn)

Address: No.5 Yiheyuan Road, Haidian District, Beijing 100871, P. R. China

Contents of this file

Figures S1 to S12

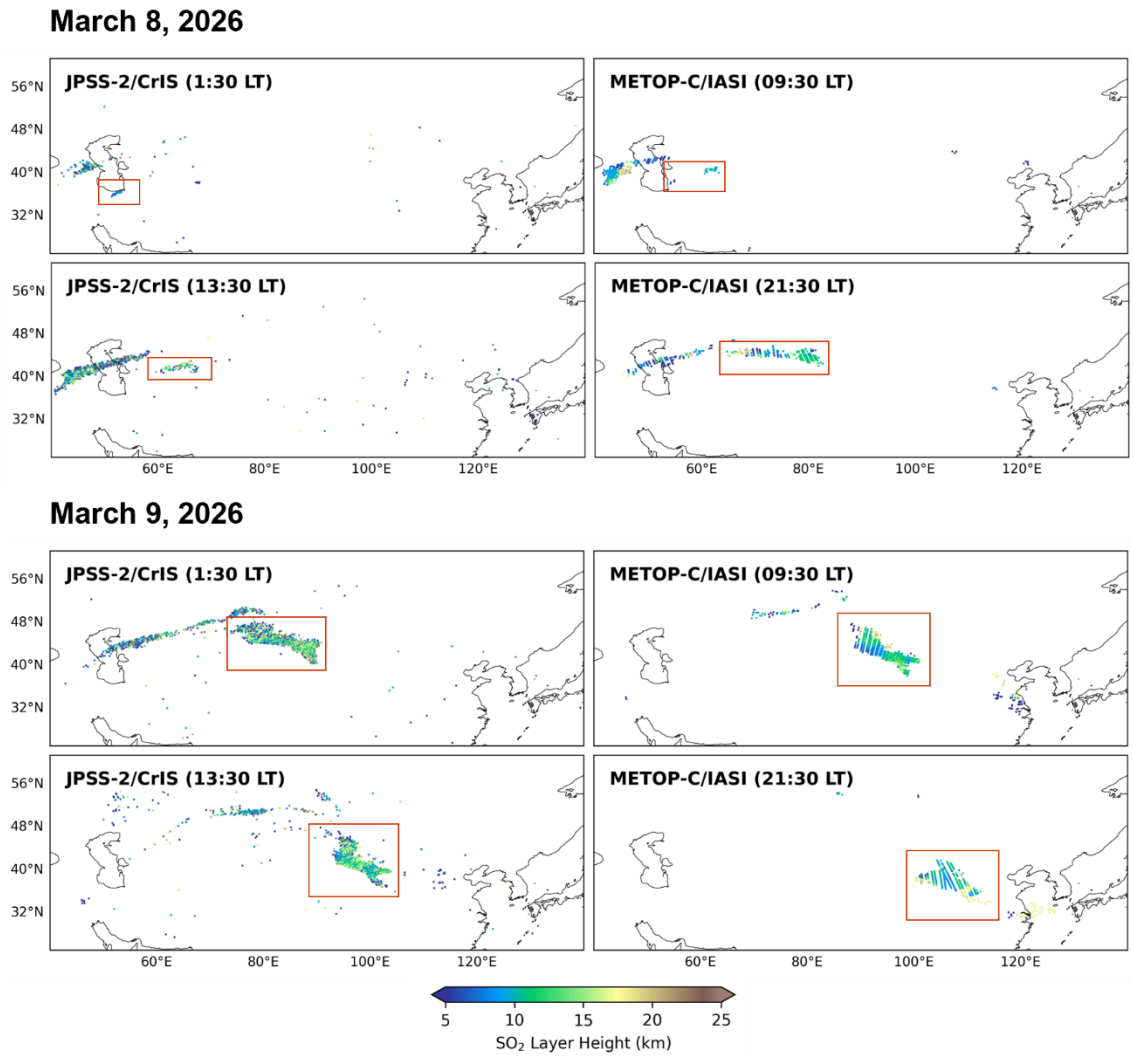

Figure S1: Spatial distribution of the estimated SO_2 layer height derived from JPSS-2/CrIS and METOP-C/IASI observations on March 8 and 9, 2026. The red boxes indicate the SO_2 plume mainly produced by the refinery explosion, corresponding to the domains used for the SO_2 mass calculations in Fig. 3. The SO_2 enhancement signals detected outside the red boxes are likely attributed to different anthropogenic sources.

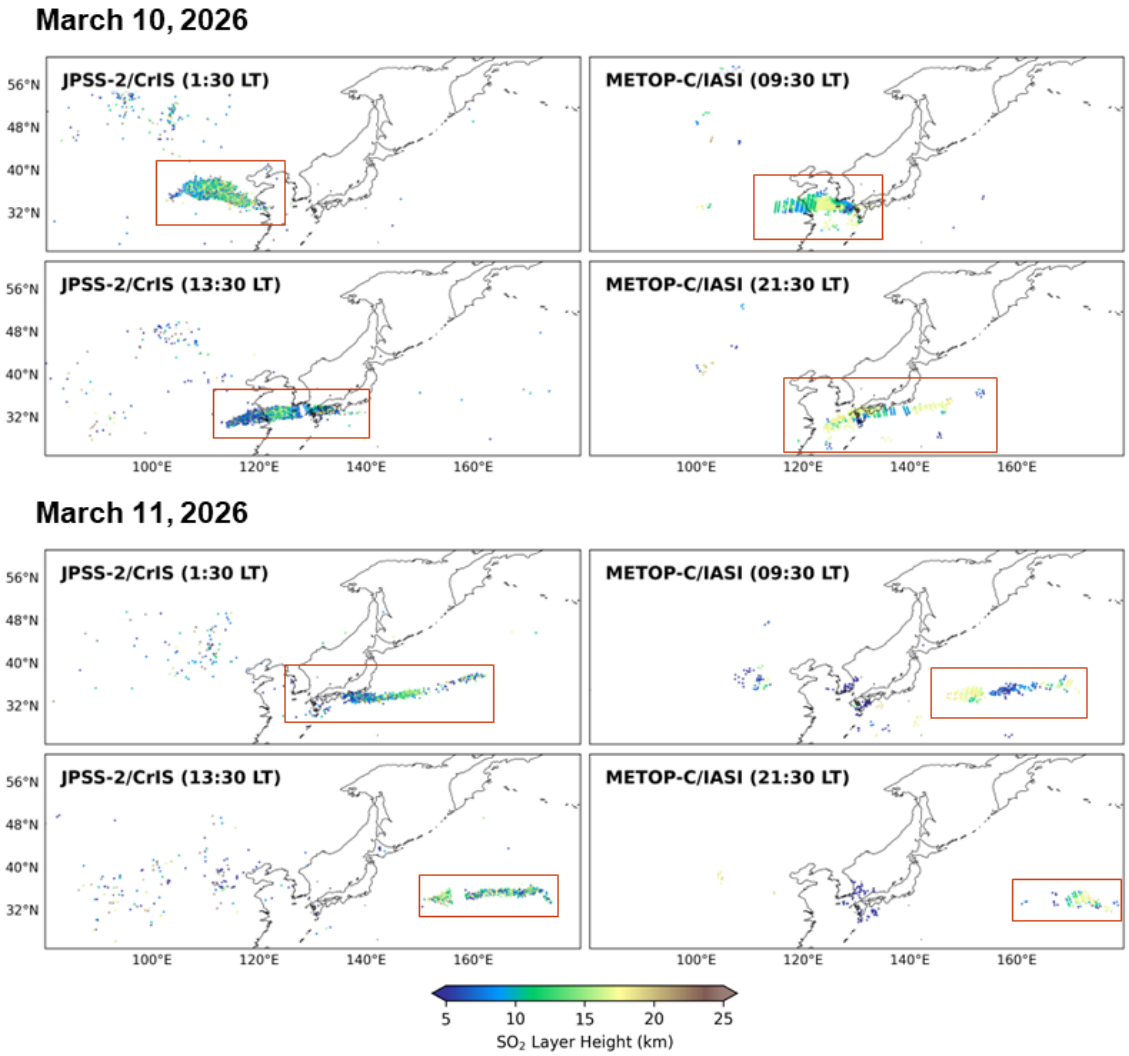

Figure S2: Spatial distribution of the estimated SO_2 layer height derived from JPSS-2/CrIS and METOP-C/IASI observations on March 10 and 11, 2026. The red boxes indicate the SO_2 plume mainly produced by the refinery explosion, corresponding to the domains used for the SO_2 mass calculations in Fig. 3. The SO_2 enhancement signals detected outside the red boxes are likely attributed to different anthropogenic sources.

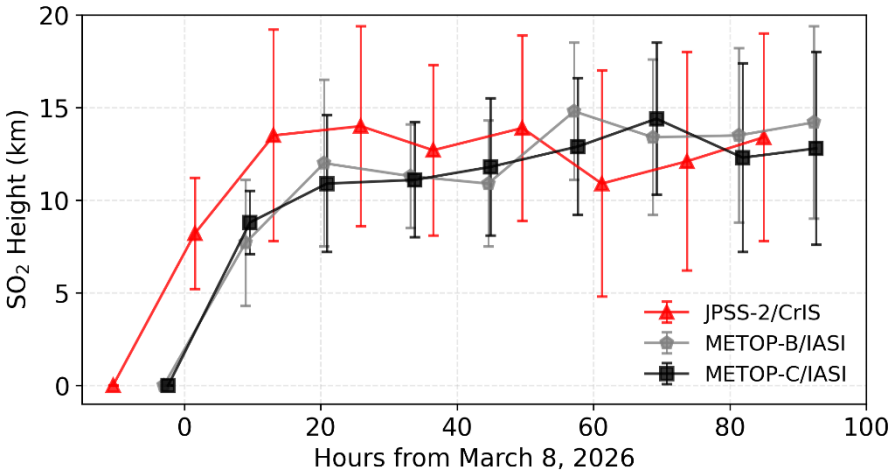

Figure S3: Time series of the mean SO_2 layer heights retrieved from CrIS and IASI following the attack, from March 8 to 11, 2026. Vertical error bars denote the standard deviations.

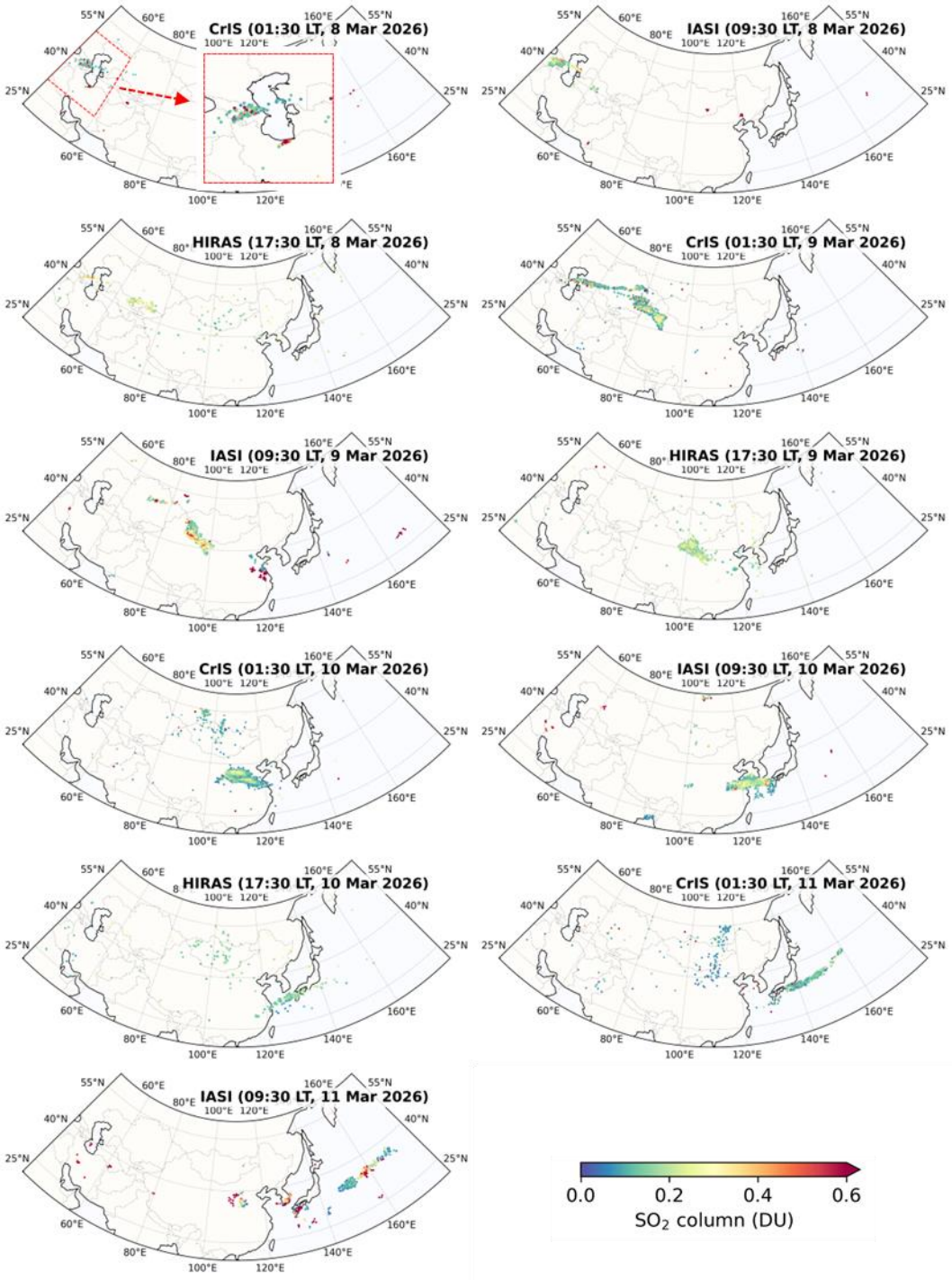

Figure S4: Spatiotemporal evolution of SO_2 total columns retrieved from the satellite constellation from March 8 to 11, 2026. For clarity, one overpass per satellite per day is shown, corresponding to local times (LT) of approximately 01:30 (CrIS), 09:30 (Metop-C/IASI), and 17:30 (HIRAS) local times (LT).

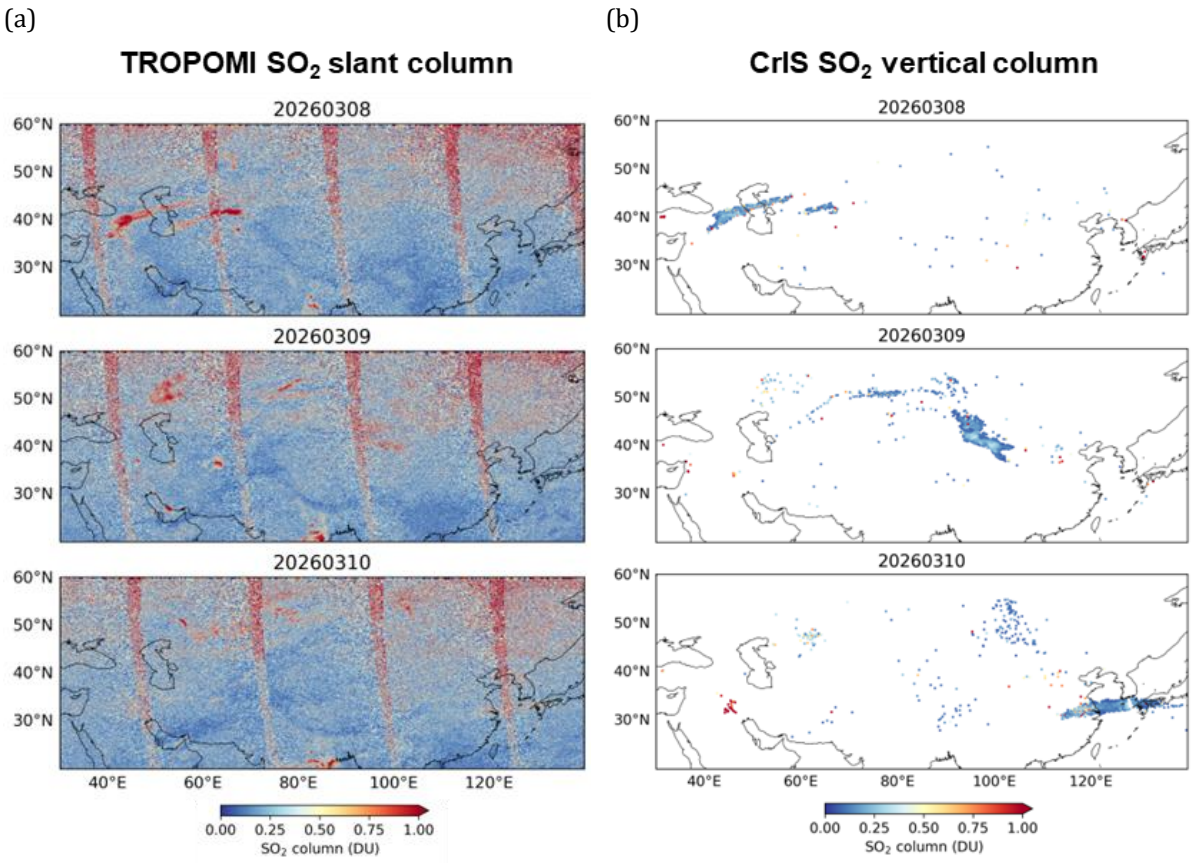

Figure S5: Comparison of (a) TROPOMI SO_2 slant columns (using the COBRA algorithm) and (b) JPSS-2/CrIS SO_2 vertical columns from March 8 to 10, 2026.

(a)

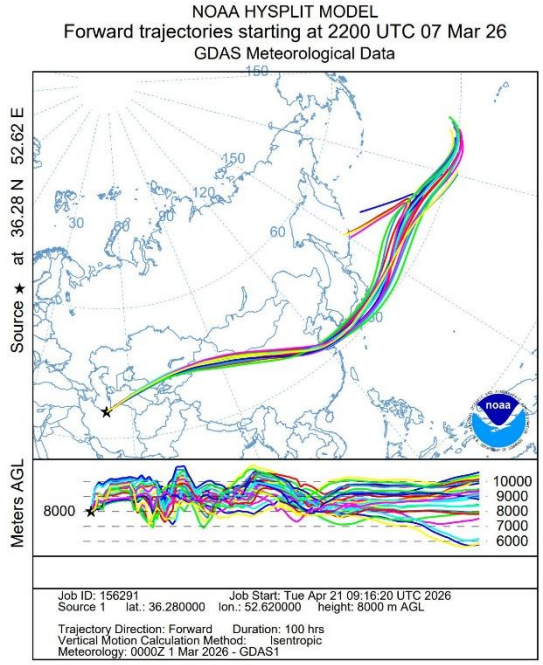

(b)

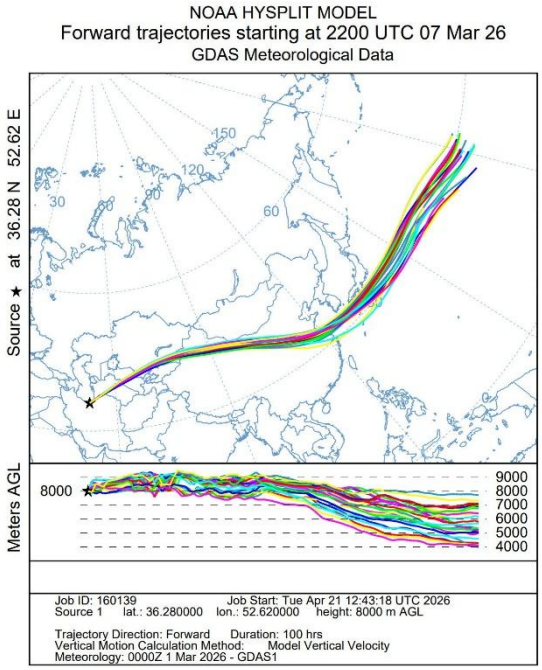

(c)

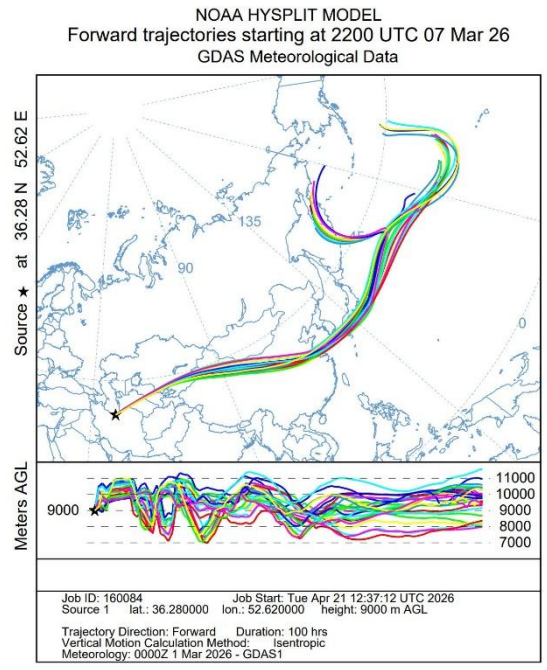

(d)

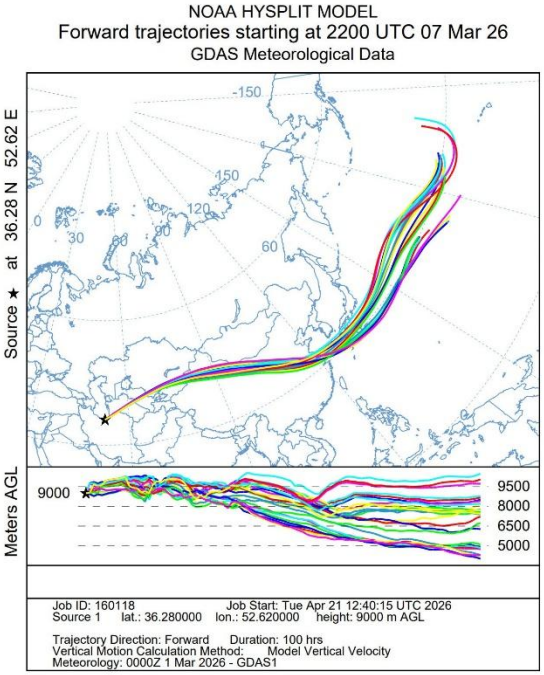

Figure S6: Simulated 100-hour forward transport trajectories of the SO_2 plume using NOAA HYSPLIT ensemble model, starting from 22:00 UTC on March 7, 2026, using different configurations: (a) 8 km initial release heights, isentropic vertical motion calculation method; (b) 8 km, model vertical velocity; (c) 9 km, isentropic; and (d) 9 km, model vertical velocity.

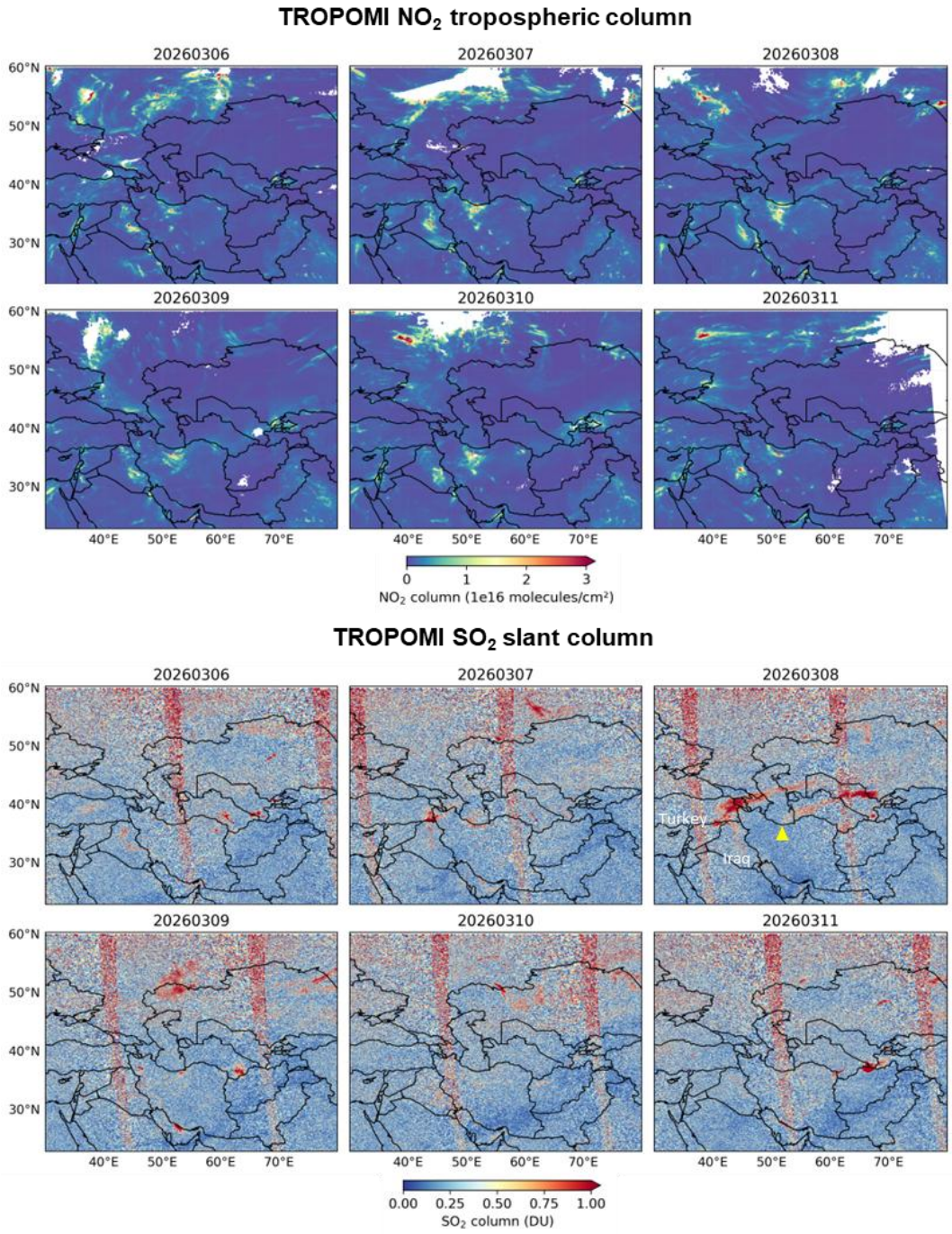

Figure S7: Spatial distributions of TROPOMI NO_2 tropospheric columns (top panels) and SO_2 slant columns (bottom panels) from March 6 to 11, 2026. The yellow triangle marks the site of the Tehran refinery explosion.

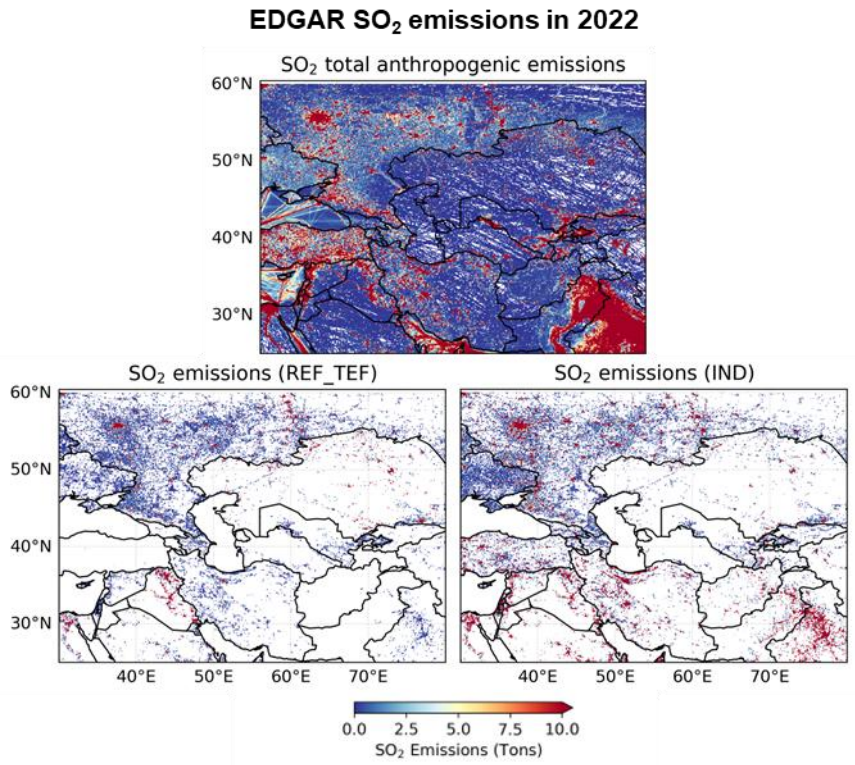

Figure S8: Spatial distribution of SO_2 emissions in 2022 based on the EDGAR (Emissions Database for Global Atmospheric Research) inventory. The panels display total anthropogenic SO_2 emissions (top), along with sector-specific emissions from refineries and energy transformation (REF_TEF, bottom left) and industrial processes (IND, bottom right).

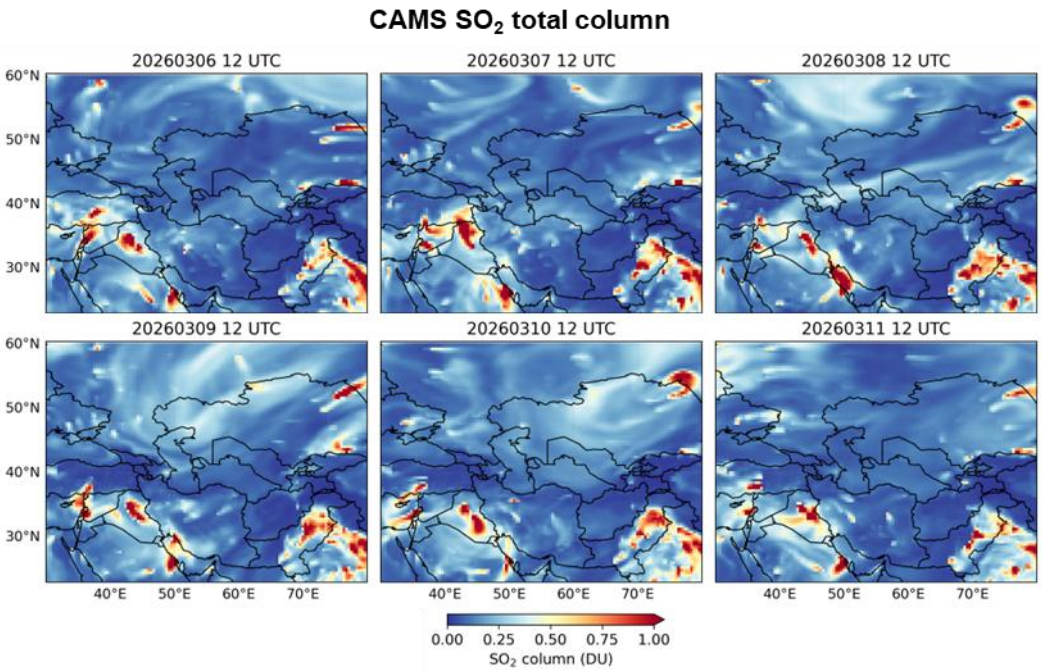

Figure S9: Spatial distributions of SO_2 total columns from March 6 to 11, 2026 at 12:00 UTC, obtained from the CAMS global atmospheric composition forecasts.

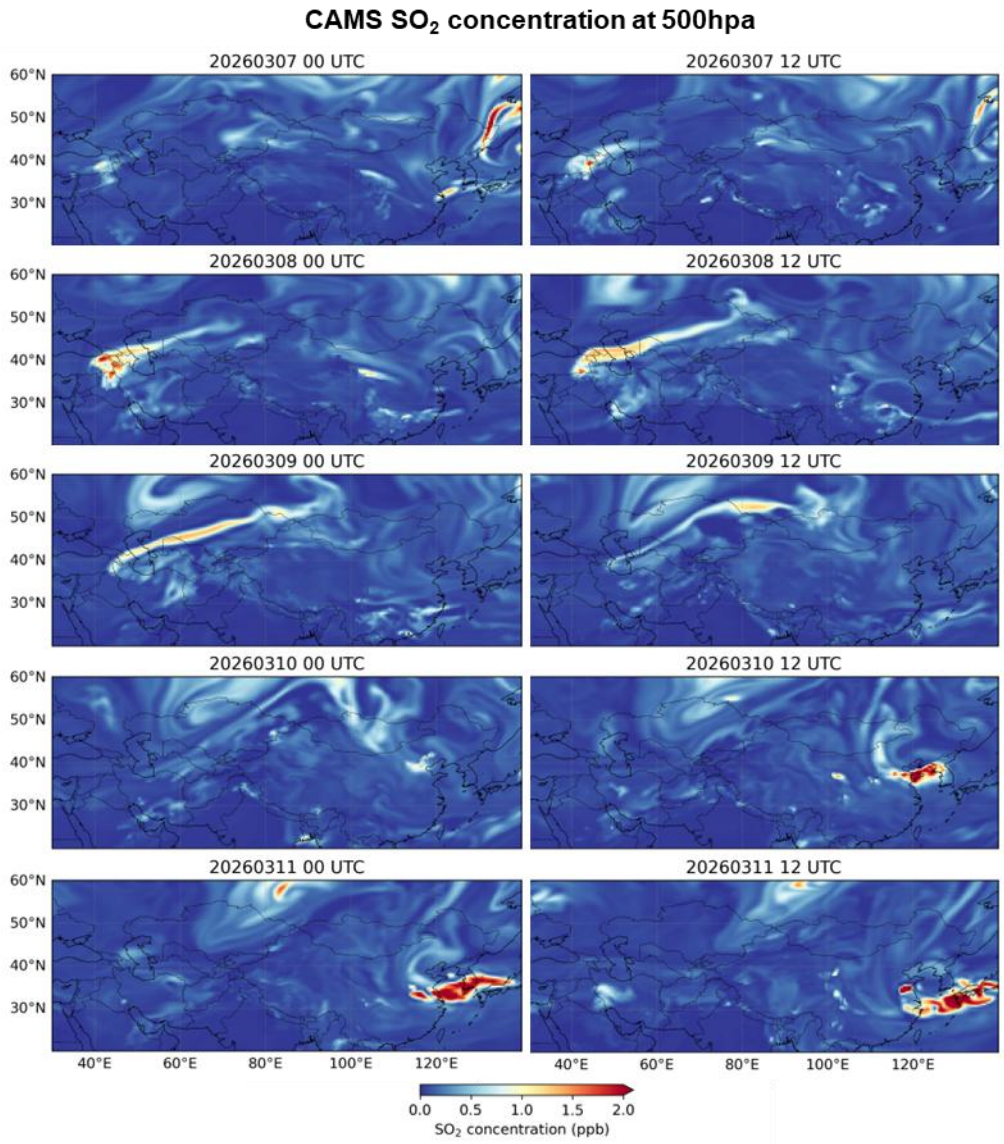

Figure S10: Spatiotemporal evolution of SO_2 concentrations at 500 hPa from March 7 to 11, 2026, based on CAMS forecasts. The left and right column panels display the model outputs at 00:00 UTC and 12:00 UTC daily, respectively.

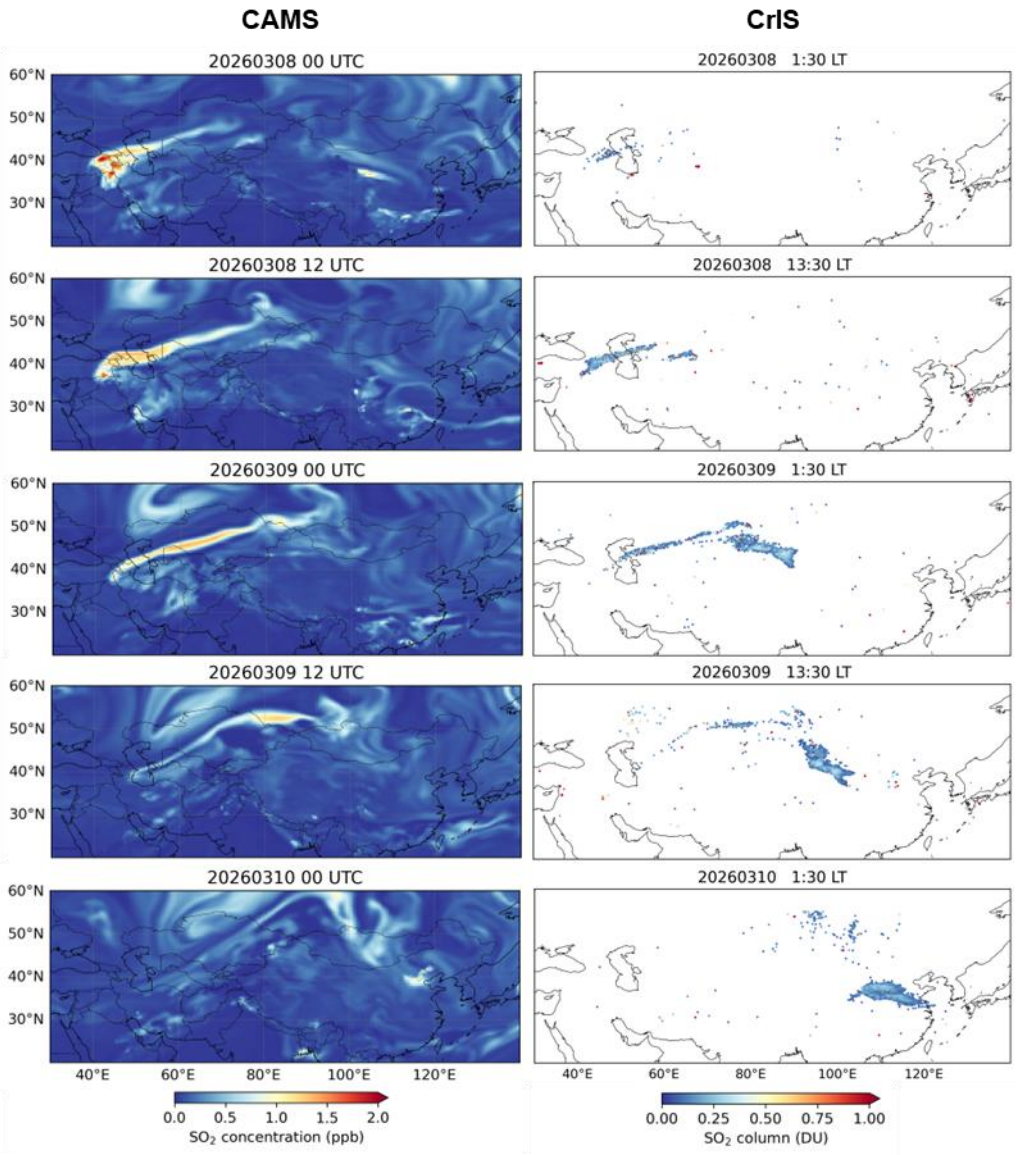

Figure S11: Comparison of CAMS SO_2 concentrations at 500 hPa (left column) and CrIS SO_2 total columns (right column) from March 8 to 10, 2026. Note the inconsistency between the model output times and the satellite local overpass times.

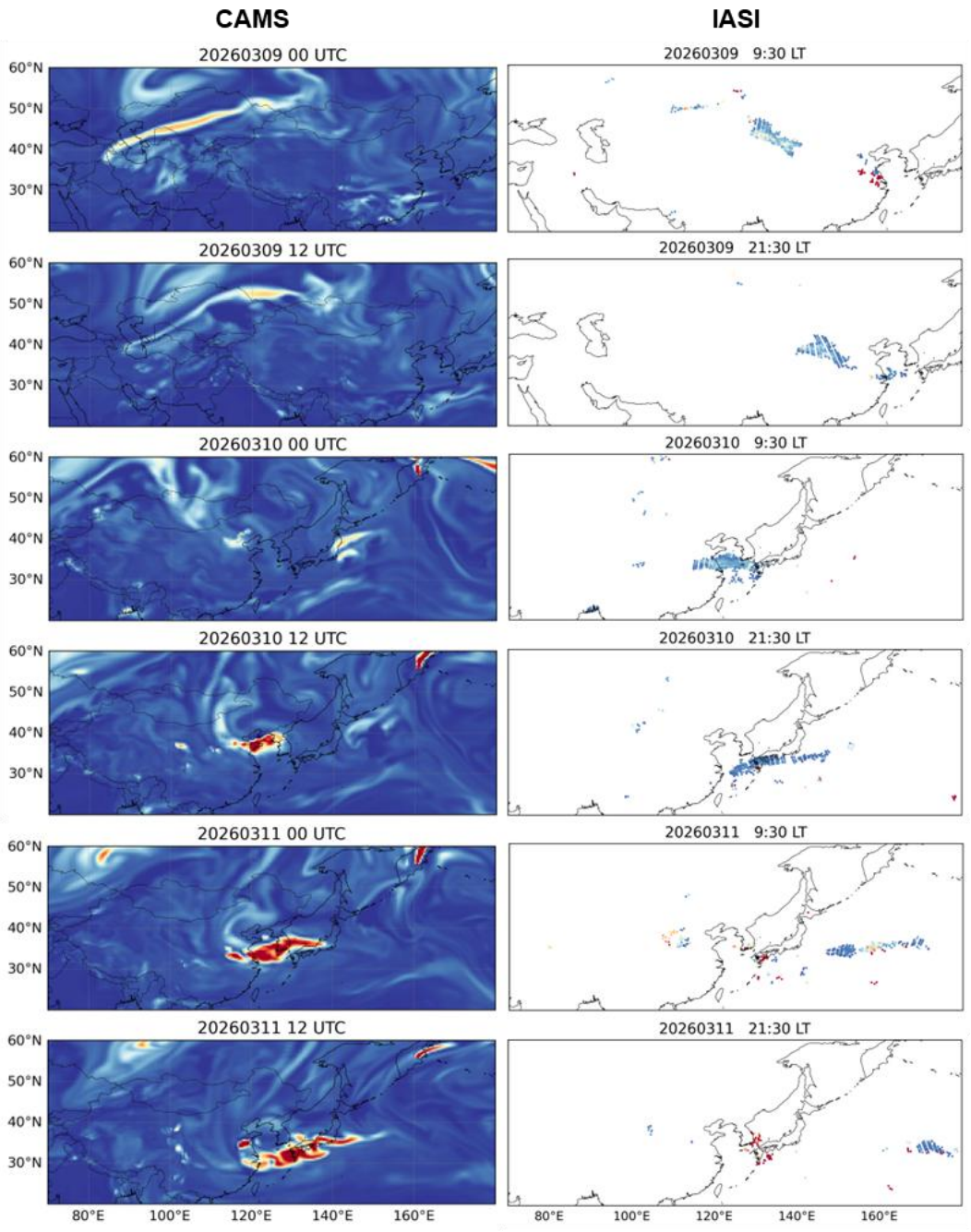

Figure S12: Comparison of CAMS SO_2 concentrations at 500 hPa (left column) and IASI SO_2 total columns (right column) from March 9 to 11, 2026. Note the inconsistency between the model output times (00:00 and 12:00 UTC) and the satellite local overpass times.